ACS APPLIED MATERIALS & INTERFACES

Research Article

www.acsami.org

Asymmetric Electrode Configuration for Enhanced Membrane Capacitive Deionization

Ayokunle Omosebi, Xin Gao, James Landon,* and Kunlei Liu*

Center for Applied Energy Research, University of Kentucky, Lexington, Kentucky 40511, United States

Supporting Information

ABSTRACT: Long-term performance of capacitive deionization (CDI) and membrane-assisted capacitive deionization (MCDI) single cells equipped with the same pristine carbon xerogel (CX) electrodes configured as the anode and cathode was investigated. Unlike CDI, which was subject to performance degradation in a short period of time, MCDI showed performance preservation during the 50 h of operation due to its ability to mitigate charge leakage from parasitic electrochemical reactions that result in carbon oxidation. Differential capacitance measurements of the used CDI and MCDI electrodes revealed shifting of the potential of zero charge (E_{PZC}) of the CDI anode from −0.1 to 0.4 V but only to 0.1 V for the MCDI anode. CDI and MCDI cells tested with electrodes having E_{PZC}s at −0.1 and 0.5 V showed strongly contrasting results depending on the anode−cathode E_{PZC} configuration. The MCDI cell configured with a 0.5 V E_{PZC} cathode and −0.1 V E_{PZC} anode displayed the best performance of all the tested cells, benefiting from increased counterion excess within the potential window, and the membrane was in-place to reject expelled co-ions from accessing the bulk.

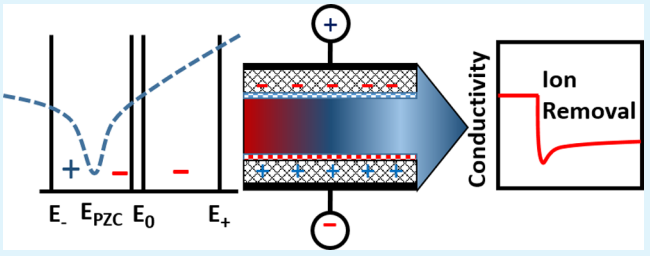

KEYWORDS: *potential of zero charge, capacitive deionization, ion-exchange membranes, carbon xerogel, carbon degradation, electrochemical impedance spectroscopy*

INTRODUCTION

Freshwater production is a serious concern as global population and the demand for freshwater continue to rise.[1−3] Presently, separation techniques like reverse osmosis (RO), electrodialysis (ED), and multistage flash distillation (MSD) are extensively employed for water desalination and freshwater production, but significant cost and energy requirements by the separation processes are prohibitive.[4−6] Capacitive deionization (CDI) is an emerging technology for clean water production from brackish sources whereby the salt ions are concentrated into the electrical double layers (EDLs) formed in highly porous electrodes.[6−13]

In CDI, counterions from the bulk solution are electrostatically transported and stored under the influence of an applied electric potential in porous electrodes of the opposite polarity. Upon relaxation of the applied potential, the ions desorb back into the flush solution, and the energy used for ion adsorption can be recovered in a manner akin to supercapacitors. Membrane capacitive deionization (MCDI) is an improvement to conventional CDI implemented by affixing ion-exchange membranes (IEMs) to the porous electrodes for a more selective ion adsorption/desorption process.[13] CDI and MCDI are schematically contrasted in Figure 1. When an electrode is polarized, it causes not only the attraction of counterions but also the expulsion of co-ions from the vicinity of the electrode. In MCDI, the membranes hinder co-ion expulsion, leading to increased flux of counterions to neutralize the co-ions and maintain electroneutrality, with the end result that fewer ions are left in solution and the performance of the desalination system is significantly increased.[14−18] MCDI has been contrasted to CDI under different testing conditions including variations in deionization potential,[18,19] electrolyte concentration,[14] and electrode−electrolyte combinations such as activated carbon (AC) with IEMs,[20] flow electrodes with IEMs,[21] and carbon nanotubes/nanofibers electrodes with IEMs.[22] In all of these investigations, MCDI outperformed CDI in the time scales used for the experiments.

CDI, like capacitors, are expected to be robust and capable of a large number of charge−discharge cycles. As such, they are typically operated at potentials that maximize electrosorption without electrochemically degrading the electrolyte. However, during long-term testing, CDI cycling results have shown performance degradation,[9] even to the extent where the performance of the CDI cell becomes inverted, i.e., a discharging response occurs when potential is applied and a charging response occurs upon relaxation of the applied potential.[23,24] The inversion effect has been attributed to progressive oxidation of the anode in the electrolyte environment that alters pore characteristics, increases electrode resistance, and exacerbates ion repulsion leading to an inverted performance.[24,25] Even at the potentials where CDI is operated, continuous cycling appears to lead to carbon electro-oxidation,

Received: April 29, 2014
Accepted: July 2, 2014
Published: July 2, 2014

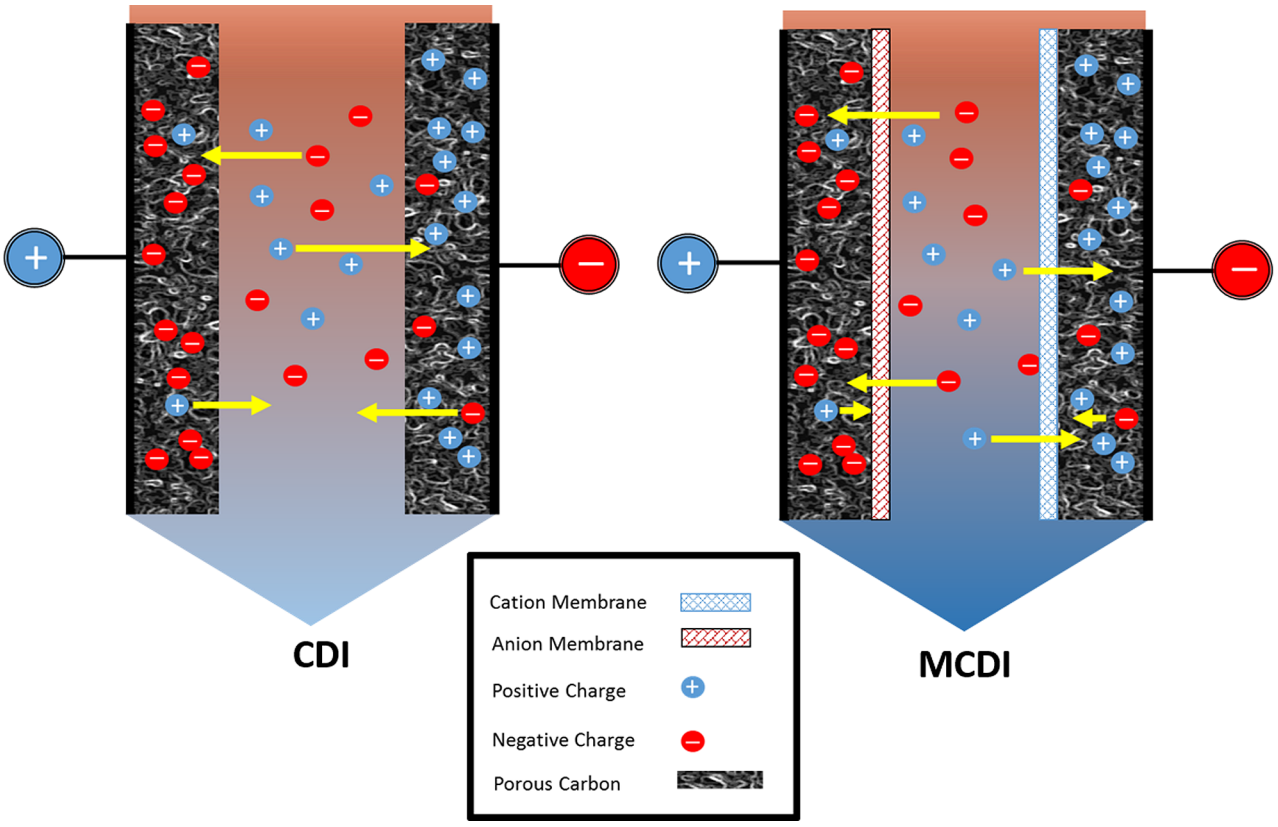

Figure 1. Schematic representation of the operation of CDI and MCDI cells. Counterions are electrostatically attracted to opposite polarity electrodes, while co-ions are expelled. Membranes in the MCDI process screen the co-ions from returning to the bulk, thus attracting more counterions to neutralize the charge.

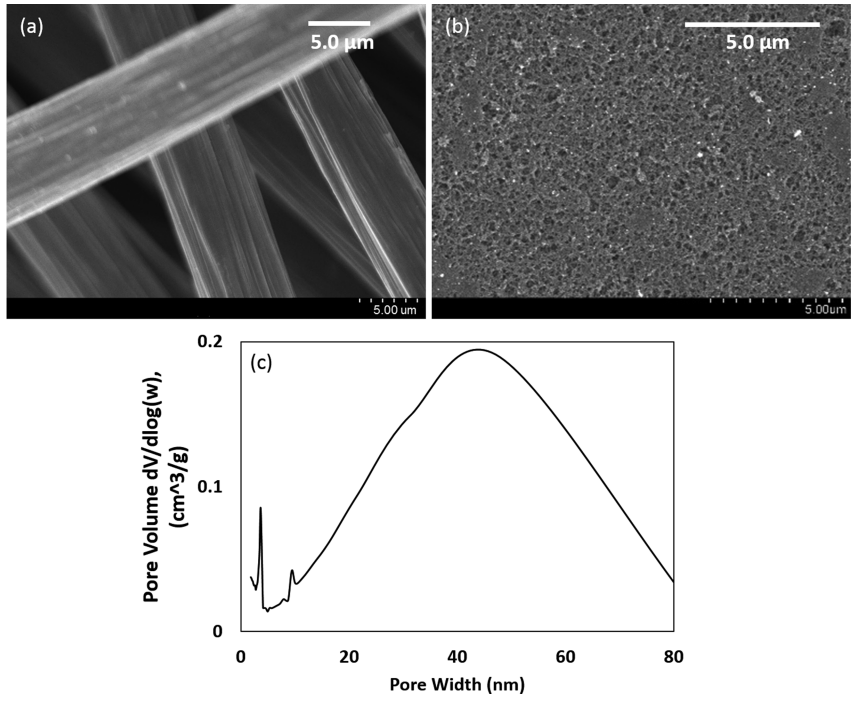

Figure 2. SEM micrograph of (a) carbon cloth and (b) resulting carbon xerogel substrate. Pore characteristics (c) highlights a predominantly mesoporous structure for the CX electrode.

and to the best of our knowledge, the impact of repeated cycling on electrode degradation has never been discussed in the context of MCDI. This paper will examine the role of the membrane for performance preservation and the mitigation of electrode degradation.

dx.doi.org/10.1021/am5026209 | ACS Appl. Mater. Interfaces 2014, 6, 12640−12649

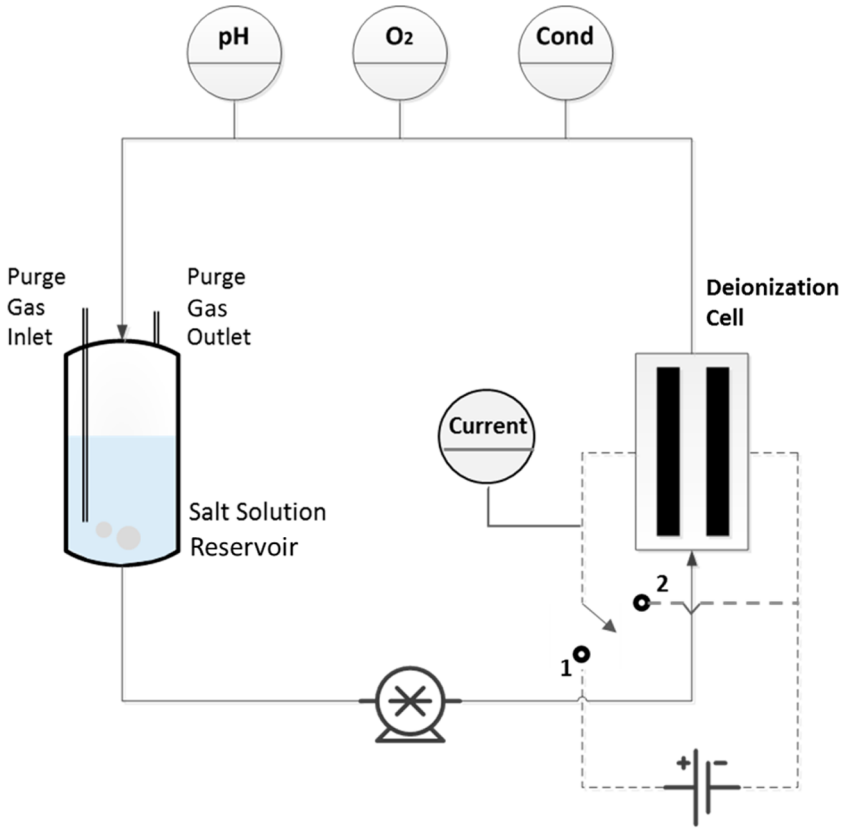

Figure 3. Capacitive deionization setup composed of a deionization cell, pH, O_2, and conductivity sensors. A 600 mL solution of 0.005 M NaCl was continuously recirculated at approximately 16 mL/min through the system.

In addition to pore characteristics, the performance of CDI cells is intricately linked to the potential of zero charge (E_{PZC}) of the electrodes. E_{PZC} is a characteristic potential where the net charge on an electrode interfacing an electrolyte is minimized. At potentials greater than the E_{PZC}, there is an excess of negative ions in the double layer, while cationic excess occurs when the electrode is polarized more negative than the E_{PZC}.[8,23,24] E_{PZC} customization via electrode functionalization has been used to boost performance in CDI cells in the past.[10,26] Distinct from previously published work on MCDI, we offer a new perspective on the synergistic effect of coupling E_{PZC} modified carbon electrodes with ion-exchange membranes.

EXPERIMENTAL METHODS

Electrode Preparation. Carbon xerogel (CX) infiltrated into woven carbon cloth substrates (fuelcellearth.com) was used as an electro-adsorbent material in this work. The xerogels were produced by mixing resorcinol with formaldehyde in a 1:2 ratio, followed by the addition of Na_2CO_3 as a catalyst in a 1 to 1500 ratio with resorcinol and, finally, water to adjust the resorcinol–formaldehyde (RF) percentage.

The mixture was magnetically stirred for 30 min and then infused into carbon cloth. The resulting substrate was subsequently immobilized and sealed between two glass slides and allowed to gelate for 24 h, followed by heat treatment at 85 °C for 24 h. The sample was then soaked in deionized water for 2 h, followed by solvent exchange with acetone for 2 h, and last dried in air for 2 h. Once dry, the sample was carbonized in a tube furnace (Thermo Scientific Lindberg Blue) at 1000 °C for 2 h in N_2 atmosphere using a 5 °C/min heating and cooling rate from room temperature to the carbonization temperature and back to room temperature after carbonization. The CX sheets were withdrawn from the furnace and stored in vacuum until required. CX sheets at this stage are designated as pristine CX electrodes. Additional details on the fabrication procedure of these CX electrodes can be found in ref 27. In particular, the CX electrodes used for performance testing in this work were made from a 40 wt % resorcinol–formaldehyde mixture. Figure 2 shows SEM micrographs (Hitachi S-4800 Scanning Electron Microscope) of the surface morphology of the starting carbon cloth material and the final CX electrode. The carbon cloth is composed of strands of fibrous carbon material, while the CX substrate had a spongy predominantly mesoporous structure evidenced by the pore-size distribution plot obtained via the BJH method (Figure 2c). Pore characteristics were examined with a Micromeritics ASAP 2020 using N_2 adsorption/desorption at 77 K.

Electrochemical Testing. A Gamry Reference 600 potentiostat/galvanostat was used for the electrochemical characterization of all the test electrodes. CX sheets resized to ~2 × 0.5 × 0.015 cm^3 (~0.02 g) were used as the working electrode, while a larger CX electrode ~3 × 4.5 × 0.015 cm^3 (~0.27 g) was used as the counter electrode. Testing was done in a three electrode half-cell setup equipped with a saturated calomel electrode (SCE) as the reference electrode. E_{PZC} information was obtained from differential capacitance measurements conducted using impedance spectroscopy. A 0.01 M NaCl solution in DI water was used as the electrolyte. EIS data was obtained by inputting a 30 mV RMS amplitude signal and nominally scanning the frequency from 0.2 to 2000 Hz. The EIS measurements were made from −0.4 to 0.8 (V vs SCE) with potential increments of 0.1 V. The specific capacitance (C) was derived from the imaginary part of the impedance spectrum (Z'') and scanning frequency (ω) according to the following equation.[15]

$$C = \left| \frac{1}{\omega Z''} \right| \quad (1)$$

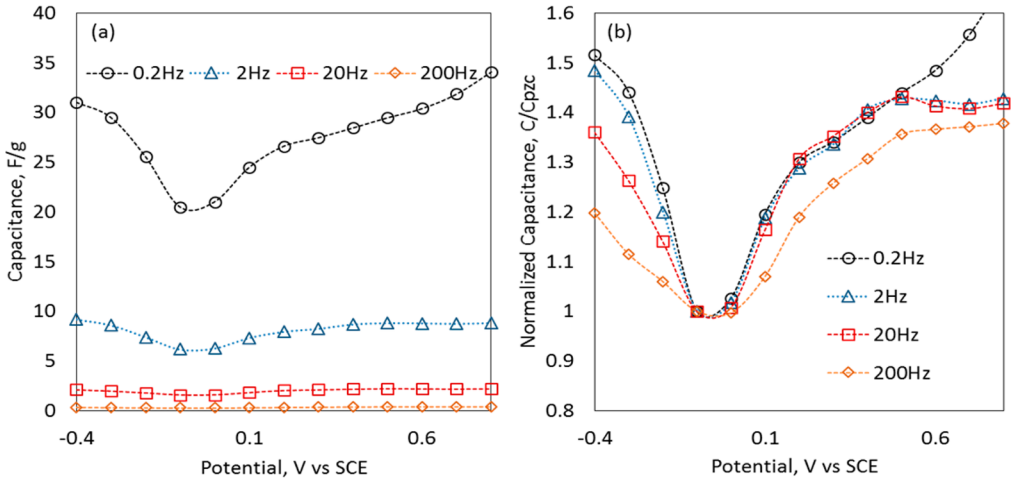

Figure 4. EIS differential capacity (a) and normalized capacitance (b) curves for pristine carbon xerogel in 0.01 M NaCl. The capacity minimum is located at ∼−0.1 V vs SCE.

Unless stated otherwise, E_{PZC} was determined from the minima of the plot of the capacitance at the minimum frequency (0.2 Hz) as a function of potential.

Deionization Performance Testing. Batch-mode capacitive deionization experiments were carried out using the test equipment shown in Figure 3 by recirculating deaerated NaCl solution contained in the reservoir through the deionization cell and back to the reservoir. The experimental setup was equipped with in-line sensors for tracking changes in conductivity, pH, dissolved oxygen, and current passed. All the sensors were connected to a Graphtec midi Logger GL220 programmed to obtain and log data at a rate of 0.2 Hz. The reservoir was continuously purged with argon gas during CDI testing. The CDI cell was connected to a DC power supply (Circuit specialist 3644 A) via a relay controlled SPDT switch that cycles potential at the CDI cell between charging (1.2 V) and discharging (short-circuit) modes. Performance cycling and SPDT switch timing were controlled using an Allen Bradley (Micrologix 100) programmable logic controller. During deionization, the SPDT switch is set to position 1 and then switched to position 2 for discharge (Figure 3). In this type of batch-mode experimental configuration, when a sizable cell potential is applied, the conductivity profile is expected to show a steady-state step difference; i.e., there should be a difference in the steady state conductivity values at pre- and post-potential application. Two deionization configurations, CDI and MCDI (Figure 1) were compared.

Within the CDI cell, the electrodes are separated by a ∼3.2 mm spacer, composed of a porous fiber glass filter (Fisherbrand P4) sandwiched between two gaskets. For MCDI, Neosepta AMX (∼0.15 mm thick) and CMX (∼0.17 mm thick) membranes were used as the ion exchange membranes and configured as shown in Figure 1. Membrane thickness was quantified using a Cen-Tech caliper equipped with a digital readout. The CMX membrane was placed adjacent to the cathode, while the AMX membrane was next to the anode with both membranes sandwiching the spacer. Deionization experiments were performed with a single pair of CX electrodes (∼1.5 g of total CX). Electrosorption capacity, Θ, of the carbon was determined from the change in conductivity of the salt solution converted to mass, normalized by the total amount of CX used.

$$\Theta = \frac{A[\Delta\sigma]VM_w}{m} \tag{2}$$

where $\Delta\sigma$ is the steady state conductivity difference between the adsorption−desorption steps calculated from the last 200 s of each step and M_w, V, m, and A are the molar mass of NaCl (g/mol), volume of the NaCl solution (L), mass of the electrode (g), and calibration parameter (8.87×10^{-3} mol·cm·mg/L·μS·g), respectively. The parameter A is the slope of NaCl concentration versus the conductivity calibration curve in mol·cm/L·μS, multiplied by a factor of 1000 to convert the NaCl amount in grams to milligrams. The charge efficiency (Λ) is the ratio of moles adsorbed converted to equivalent charge using Faraday's constant (F) compared to the charge passed during the adsorption step calculated from the integral of the current profile during the adsorption step.

$$\Lambda = \frac{AFV[\Delta\sigma]}{Q} \times 100 \tag{3}$$

RESULTS AND DISCUSSION

Potential of Zero Charge of Fabricated CX Electrodes, E_{PZC}. The E_{PZC} is a fundamental material property of the double layer interface, where there is no net charge on the surface of the electrode. For CDI operation, this parameter is critical because electro-adsorption occurs when the electrode is polarized away from the E_{PZC}, i.e., $|E - E_{PZC}| > 0$ for net charge/ion adsorption to occur, where E is the potential applied to the electrode.[8] For liquid electrodes like Hg that are ideally polarizable over a range of potentials, E_{PZC} is determined from electro-capillary measurements. However, the surface tension of solid electrodes is not so easily measured. Therefore, E_{PZC} can be determined instead from immersion measurements[28] or capacity measurements in dilute electrolyte solutions.[29,30] E_{PZC} was determined here for CX samples via differential capacitance minimum measurements using EIS. Capacitance was plotted as a function of potential and at different frequencies for pristine CX electrodes as shown in Figure 4a. $E_{PZC\text{-}CX}$ was −0.1 ± 0.05 V vs SCE, and capacitance increased with decreasing frequency (Figure 4a), similar to previously published results for nanoporous carbon electrodes (prepared from TiC via chlorination) in an acetonitrile electrolyte.[31] The frequency dependence of capacity is a byproduct of the complexity of the pore structure, which restricts ion transport and increases the effective diffusion time.[32] The transport limitation becomes better resolved at lower frequencies, where the perturbation signal matches the time scale of the process. In addition to pore access restrictions, capacitance may be further diminished by overlapping of the double layer within micropores.[13] Nevertheless, a characteristic capacity minimum was repeatedly observed for all represented frequencies as shown in Figure 4b, which is a normalized capacity plot. However, Figure 4b also shows better resolved capacity curves (deeper curves) with decreasing frequency, and as such, low frequencies should be

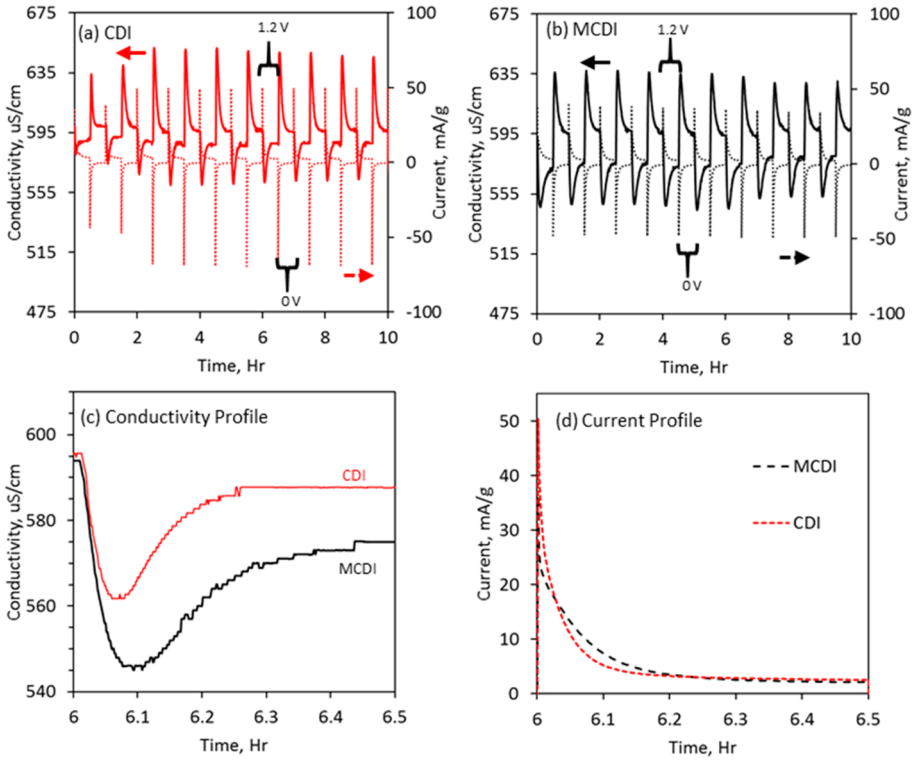

Figure 5. CDI (a) and MCDI (b) results during the first 10 h of operation and obtained by recirculating 600 mL of a ~0.005 M NaCl stream through the CDI cell at a rate of ~16 mL/min. Neosepta AEM and CEM were used as anionic and cationic membranes for the MCDI tests, respectively, and performance testing was done in a constant voltage mode by cycling between 1.2 and 0 V. All cells were configured with pristine CX electrodes. Zoomed-in conductivity (c) and current (d) profiles during cell charging−deionization are also shown.

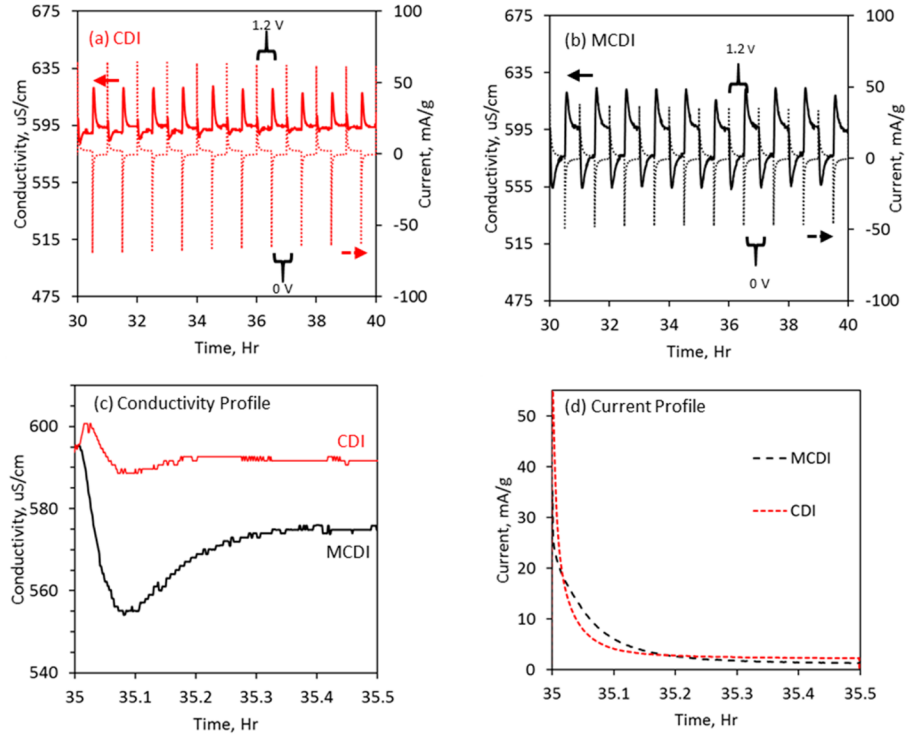

Figure 6. CDI (a) and MCDI (b) results after 30 h of operation and obtained by recirculating 600 mL of a ~0.005 M NaCl stream through the CDI cell at a rate of ~16 mL/min. Neosepta AEM and CEM were used as anionic and cationic membranes for the MCDI tests, respectively, and performance testing was done in a constant voltage mode by cycling between 1.2 and 0 V. All cells were configured with pristine CX electrodes. Zoomed-in conductivity (c) and current (d) profiles are also shown. Inversion spikes observed in the CDI conductivity profiles.

used for the E_{PZC} location. All subsequent E_{PZC} results to follow are based on capacity measurements at 0.2 Hz.

Cycling Performance of CX Electrodes in CDI and MCDI Cell Configurations. Capacitive deionization experiments were carried out by continuously recirculating 600 mL of dilute 0.005 M NaCl solution at ~16 mL/min through the experimental setup described in Figure 3. Neosepta AEM and CEM were used as anionic and cationic membranes for the MCDI tests. Performance testing was done in a constant voltage mode by cycling between 1.2 and 0 V (short circuit) every 30 min; i.e., a full cycle lasts 1 h. Performance data was logged every 5 s, and pristine electrodes were configured as anode and cathode for both CDI and MCDI.

Typical batch-mode deionization profiles (Figure 5) were obtained for both CDI and MCDI; i.e., there is a steady-state solution conductivity difference between the charging (1.2 V) and discharging (short-circuit) states. Figure 5a,b shows the conductivity and current profiles for CDI and MCDI during the first 10 h of operation. Selected deionization curves are shown in Figure 5c,d. During the 10 h operation window, the average conductivity drops were 8.2 and 19.3 μS/cm for the CDI and MCDI cells, respectively. The increased performance from incorporating IEMs into the CDI process is consistent with results from other authors.[15−19]

Adding these membranes also resulted in increased ohmic resistance, evidenced by a reduction in the initial current at the onset of charging and discharging. Given that the membranes provide facile transport of counterions to their respective electrodes, the ohmic resistance encountered is more likely due to interfacial resistance between the membrane and the electrode. As illustrated in Figure 5d, the nominal initial current density during the charging cycles were ~50 and ~34 mA/g, respectively, for the CDI and MCDI cells. After ~3 min of operation, the current profiles intersect, and more current flows through the MCDI cell. The total charge passed in the experimental time window is ~9 Coulombs/g for both CDI and MCDI, which implies the ohmic drop in the MCDI is compensated by increased removal of counterions from the bulk and a further drop in conductivity for the MCDI cell (evidenced in Figure 5c).

Due to their similarity to supercapacitors, the CDI cells were expected to have high cycling ability in the water treatment environment. To verify the long-term performance, CDI and MCDI cells were further cycled to observe their material behavior. Figure 6 shows the conductivity and current profiles of the CDI and MCDI cells after 30 h of operation. In contrast to the results in Figure 5, the performance of the CDI cell became significantly diminished. Furthermore, a spike in conductivity was observed for the CDI cell at the onset of each application of the charging potential (Figure 6a,c). Similar results have been observed with activated carbon by Cohen et al., during long-term CDI operation. This spike was interpreted as the inversion spike and is a byproduct of degradation of the anode via electro-oxidation.[24] Interestingly, the CDI current profile was still maintained (Figure 6a,d). In addition to counterion charge storage, some of the potential supplied to the cell for adsorption is being used for charge expulsion and electrode reaction (material degradation), thus decreasing the amount of charge actually stored. In comparison, the conductivity drop for the MCDI cell was maintained at ~19.0 μS/cm.

Cycle to cycle electrosorption capacities and charge efficiency were plotted (Figure 7) for CDI and MCDI for the duration of

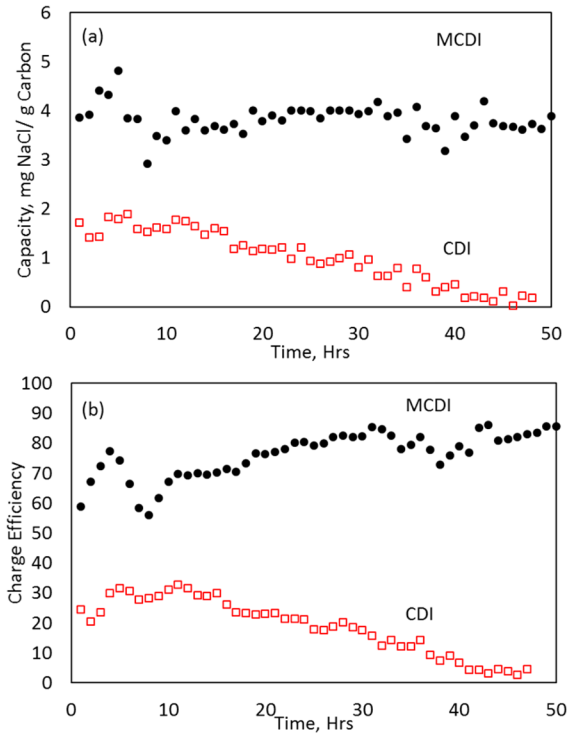

Figure 7. Long-term MCDI and CDI electrosorption capacity (a) and charge efficiency (b). Degraded and preserved performances were observed for the CDI and MCDI cells, respectively.

the experiments. For CDI, the deionization capacity gradually degraded (almost linearly) over time. The maximum observed capacity was ~2 mg NaCl/g carbon. In contrast, the MCDI cell maintained a nominal capacity of ~3.5 mg NaCl/g C during the test period. Charge efficiency in the first 10 cycles was ~30% for the CDI cell but degraded over time with continued operation. For MCDI, the nominal efficiency was ~80% during this testing period. During CDI and MCDI operation, cycle-to-cycle current profiles are similar (Figures 5d and 6d), while the conductivity and consequently electrosorption capacity vary with continued operation. Since the efficiency is a normalization of the charge passed by tracking changes in salt concentration to charge passed by tracking the current, the efficiency likewise diminishes for the CDI system with degraded conductivity. In comparison, the charge efficiency is more invariant for the MCDI system. These results show that, in addition to boosting performance, MCDI operation has an added benefit of performance preservation.

Degradation in performance can be attributed to changes in the liquid electrolyte or solid electrode, because both phases are involved in the formation of the double layer, wherein the charges removed from solution are to be stored. However, given the lack of variation in the steady state conductivity of the discharged electrolyte (Figures 6 and 7), loss of deionization performance can be primarily attributed to changes in the electrode with continued cycling.

Electroxidation in CDI and MCDI Cell Configurations. In order to track changes to the electrodes capability for charge storage, E_{PZC}s of the used CDI and MCDI electrodes were determined and compared to that of a fresh pristine electrode. The used test electrodes were examined after 25 and 50 cycles (hours) in two separate experiments. During the measurement of E_{PZC}, the electrodes were first withdrawn from the

dx.doi.org/10.1021/am5026209 | ACS Appl. Mater. Interfaces 2014, 6, 12640−12649

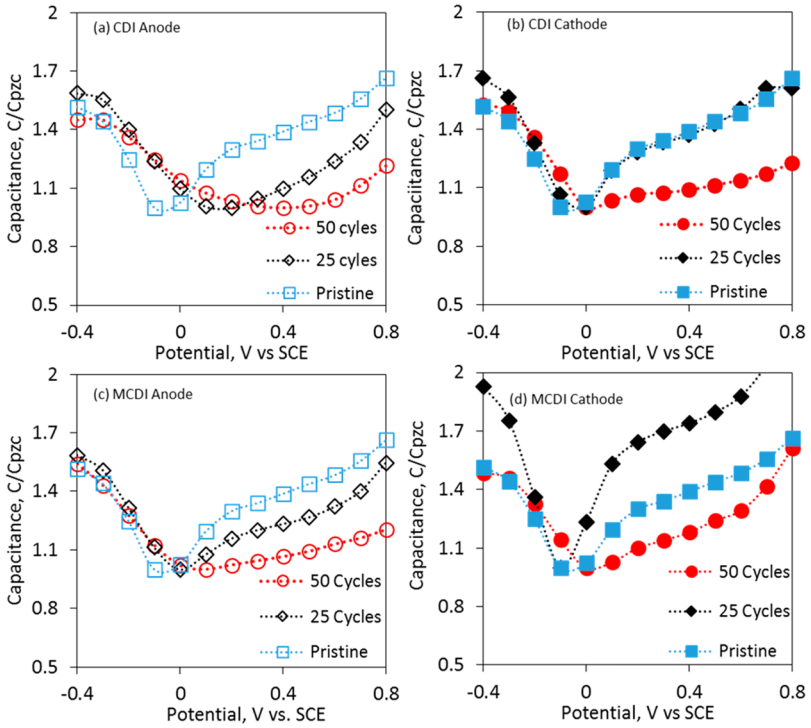

Figure 8. E_{PZC} examination of used (a) CDI anode, (b) CDI cathode, (c) MCDI anode, and (d) MCDI cathode.

deionization cells; then, EIS was performed in an electrochemical half-cell setup. All measurements are made relative to an SCE reference electrode. Figure 8 shows the differential capacity measurements obtained in 0.01 M NaCl for used CDI and MCDI electrodes. E_{PZC} is the potential where the capacity is minimized. In Figure 8a, E_{PZC} for the CDI anode shifted from ∼−0.1 to ∼0.2 V (i.e., 0.3 V shift) after 25 h (cycles) of operation and to ∼0.4 V (i.e., 0.5 V shift) after 50 h. In comparison, the MCDI anode shifted to 0 V (i.e., 0.1 V shift) after 25 h and then to 0.1 V (i.e., 0.2 V shift) after 50 h which is 0.3 V less than that of CDI. However, E_{PZC} at the CDI and MCDI cathodes were only marginally shifted by 0.1 V at the end of the 50 h continuous cycling period which indicates an incremental limitation of CDI performance by the anode.

While the potential applied to a CDI cell should ideally be utilized for just charge storage within the double layer, in reality, it is also used to overcome ohmic (electronic and ionic) and mass transport resistances to delivering charged species to the double layer during the deionization process. Furthermore, the presence of electrochemical reactions complicates the CDI process. The mechanism for carbon oxidation is possibly linked to the dissolved oxygen in the CDI system. Bouhadana et al. suggested the presence of the parasitic electrochemical reduction of dissolved oxygen and provided evidence via XPS results in conjunction with reduced charge leakage when their CDI cells, charged at 1.1 V, were purged with nitrogen instead of air.[23,33] The redox reactions are

$$O_2 + H_2O + 4e^- \rightarrow 4OH^- \quad (4)$$

$$C_{surface} + H_2O \rightarrow C{=}O_{surface} + 2H^+ + 2e^- \quad (5)$$

Dissolved oxygen content was tracked during the deionization experiments, and the experimental data plotted in Figure S1 (Supporting Information) shows variation in dissolved oxygen during CDI operation. The trend is such that, during cell charging, the dissolved oxygen content diminishes, which is consistent with O_2 consumption at the cathode, and returns to its original value upon discharge. When O_2 reduction at the cathode and carbon oxidation at the anode form a redox couple, over time more oxidative groups will form on the carbon anode, shifting E_{PZC} to more positive potentials, which will explain the more dramatic E_{PZC} shift observed in Figure 8a. FTIR spectra showing the formation of functional groups, particularly on the used CDI anode, are presented in Figure S1, Supporting Information.

Conversely, the incorporation of the membrane for MCDI can act as a barrier to limit O_2 access to the electrode (Figure S2, Supporting Information), which in-turn will limit oxidation at the anode, and reduce the extent of E_{PZC} shifting as per Figure 8c results. Previous work by Ogumi et al. demonstrated that the diffusivity of oxygen in solid polymer electrolytes like Neosepta and Nafion membranes is up to 2 orders of magnitude less than in water.[34] In addition, while the incorporation of the membrane would effect a voltage drop, the potential available for side reactions would also be likewise diminished. A consequence of increased resistance of reactions is reduced charge leakage (Figure S3, Supporting Information).[35]

Figure 9 is an illustration of the impact of the location of E_{PZC} on the performance of a CDI cell. The represented charges show excesses in the space-charge regions in relation to E_{PZC} with the double lines indicating the region between the anode and cathode containing the electroneutral bulk electrolyte. Having a charge excess, for example, in cations, implies that $d\Gamma^+ > d\Gamma^-$, where $d\Gamma$ represents infinitesimals of the ions. Figure 9a represents the start of CDI operation with similar CX electrodes configured as the anode and cathode. At this point, the CDI cell can be considered symmetrically configured because the E_{PZC} is the same for both the anode and cathode. This was the scenario at the start of our experiments. E_0 is the short-circuit potential, while E_+ and E_- are the potentials

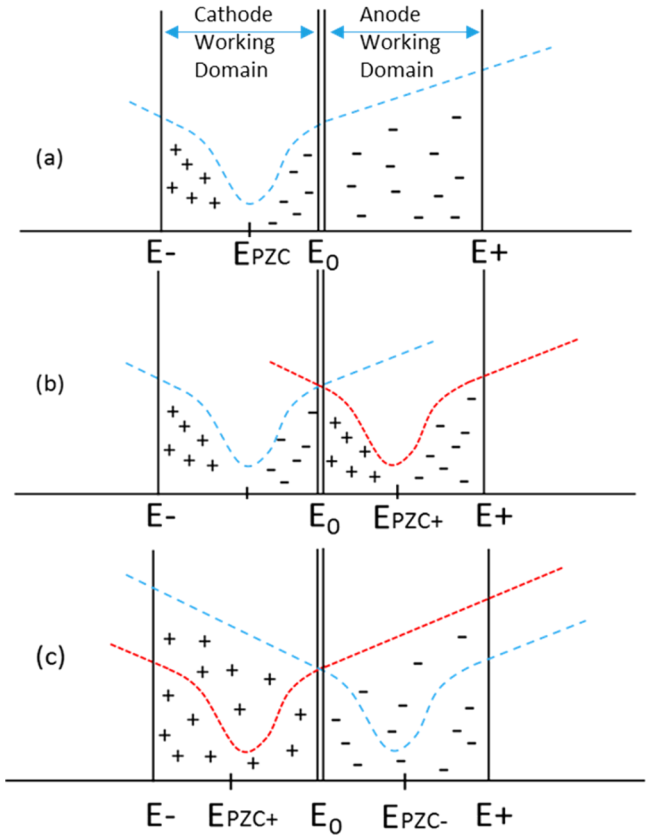

Figure 9. Representation of the effect of E_{PZC} on deionization. E_0 is the short-circuit potential, while E_+ and E_- are the potentials applied to the anode and cathode, respectively, such that $E_+ - E_-$ is the total potential applied during desalination. When the same pristine electrode (same E_{PZC}) is used as anode and cathode (a), there will be significant co-ion expulsion when the cathode is polarized from E_0 to E_-. When asymmetric electrodes with E_{PZC+} and E_{PZC-} are configured as anode and cathode (b), there is significant co-ion expulsion at both anode and cathode. If E_{PZC+} and E_{PZC-} were instead, respectively, configured as cathode and anode (c), then repulsion becomes less insignificant.

applied to the anode and cathode, respectively, such that $E_+ - E_-$ is E_{tot}. E_{tot} is the total potential applied during desalination (1.2 V during our experiments). Typical E_0, E_-, and E_+ values are ~0.2, −0.5, and 0.7 V vs SCE, respectively, and were obtained for CX electrodes from a three-electrode setup with a quiescent electrolyte whereby a potential of 1.2 V was applied across similarly sized anode and cathode, and all potentials were measured against an SCE reference.[10] E_{PZC} for pristine CX electrodes is −0.1 V vs SCE.

During deionization, the cell is polarized from E_0 to E_+ for the anode and to E_- for the cathode. When $E_- < E_{PZC} < E_0$ as is the case in Figure 9a, E_{PZC} is considered as being in the working domain of the cathode.[24] Consequently, the charging potential will be used first for co-ion expulsion and then for counterion adsorption during charging at the cathode, with the net effect that there is a reduced driving force for counterion adsorption at the cathode. At the anode, E_{PZC} is outside of the anode working domain, which implies that, in the transition from E_0 to E_+, the applied potential significantly goes toward counterion adsorption. Although such a cell as in Figure 9a was initially symmetrically configured with respect to E_{PZC} at the anode and cathode, its operation will be asymmetric due to the E_{PZC} location vs E_0, E_+, and E_- and further complications by inequalities in Na^+ and Cl^- transport numbers. With regards to symmetry, two distinctions, (1) configuration and (2) operation, are made. Configuration symmetry is defined here as having the same E_{PZC}, while operational symmetry is defined in the context of E_{PZC} relative to the working domain, such that $E_{PZC} = E_0$ is a key requirement for operational symmetry.

During long-term operation, E_{PZC} shifting occurs albeit to a greater extent for the anode than the cathode as shown in Figure 8 results. With different E_{PZC}s, cell configuration is now asymmetric. The performance of a cell is illustrated in Figure 9b, where E_{PZC+} is now in the anode working domain and E_{PZC-} remains in the cathode working domain. Here, co-ion repulsion becomes significant on both electrodes and can lead to a situation where no net adsorption occurs, when charge is equally distributed for repulsion and adsorption. Furthermore, because the initial event after potential application is co-ion expulsion, an inverted conductivity response ensues as shown in Figure 6 CDI results. However, if an oxidized electrode is configured as the anode and a pristine electrode as the cathode, the situation as illustrated in Figure 9c occurs. Both E_{PZC}s are now outside their respective potential windows, and the applied potential will be used more effectively for counterion storage.

Asymmetric Electrodes in CDI and MCDI Operation. Asymmetric configuration was explored by pairing electrodes with E_{PZC} at ~0.5 V and pristine electrodes (E_{PZC} at ~−0.1 V) for CDI and MCDI experiments. The capacity curves for the two electrode types are shown in Figure 10a, where Ox and Pr denote the oxidized and pristine electrodes, respectively. The following nomenclature is henceforth adopted: CDI-1 (anode = Ox, cathode = Pr), CDI-2 (anode = Pr, cathode = Ox), MCDI-1 (anode = Ox, cathode = Pr), and MCDI-2 (anode = Pr, cathode = Ox). Short-term performance tests were accomplished with the asymmetrically configured electrodes in CDI and MCDI cells, and the performance results are shown in Figure 10b,c.

In Figure 10b, the conductivity profiles for the asymmetric CDI and MCDI cells are shown, and the initial conductivity (σ_0, ~600 μS/cm) is clearly outlined. Configuration 1 cells (MCDI-1 and CDI-1) are similar to the cell configuration in Figure 9b, while configuration 2 cells (MCDI-2 and CDI-2) are similar to the configuration illustrated by Figure 9c. For the CDI cells, when a charging potential of 1.2 V is applied, their trends are consistent with the predictions from Figure 9b,c, such that, when both E_{PZC}s are in their respective working domains (CDI-1), performance is significantly worse, and conductivity inversion occurs from co-ion expulsion. Increased performance was observed for CDI-2 ($\Delta\sigma$, ~24 μS/cm), even in comparison to the CDI and MCDI cells from Figure 5 results with corresponding drops in conductivity of ~8.2 and ~19.3 μS/cm, respectively. Figure 5 CDI and MCDI cells are hence referred to as CDI-0 and MCDI-0. These results show a strong dependency on interfacial configuration, as performance can be significantly increased by using the electrochemically oxidized CX as the cathode and the pristine CX as anode. Notwithstanding, the configuration 1 type assembly, MCDI-1, still showed no inversion but a positive drop in conductivity (~8.0 μS/cm), albeit reduced in comparison to MCDI-0. MCDI-2 had the largest drop in conductivity (~34 μS/cm) of all the tested MCDI and CDI cells, indicating a synergistic benefit from coupling asymmetric electrodes with IEMs. In contrast to CDI-1, MCDI-1 operation maintains a conductivity drop due to the ion selectivity of the IEMs. The expelled co-ions are rejected from traversing the membranes into the bulk

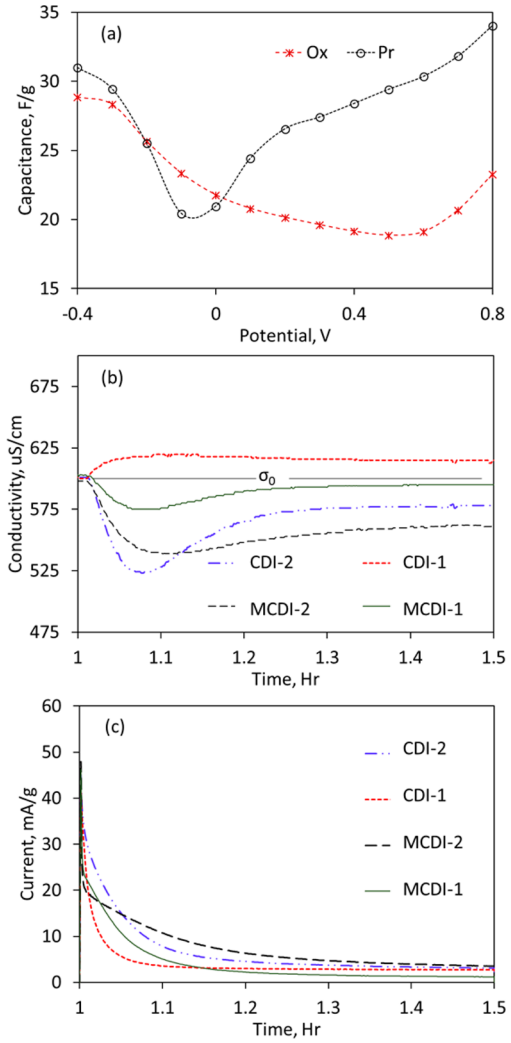

Figure 10. Electrodes (a), conductivity (b), and current (c) profiles for tested asymmetric CDI and MCDI cells. CDI-1 is configured with an oxidized anode and pristine cathode, CDI-2 with pristine anode and oxidized cathode, MCDI-1 with oxidized anode and pristine cathode, and MCDI-2 with pristine anode and oxidized cathode.

solution but are instead balanced by counterions that pass through the membrane. Since a similar process occurs at both electrodes, electroneutrality is still preserved in the bulk solution. When the cells are configured as in CDI-2 and MCDI-2, there is an excess of counterions and fewer co-ions in the EDL, implying more attraction of counterions. The co-ions expelled upon charging in MCDI-2 are still mediated by the function of the membrane, and the net result is a further reduction of ions in the bulk. The current profiles (Figure 10c) corroborate the performance results for CDI-2 and MCDI-2 in Figure 10b, with a slower current decay indicative of larger charge storage. While CDI-1 showed a typical charging current profile, there was no net deionization due to mismatched anode and cathode E_{PZC} locations.

The modification from MCDI-0 with similar pristine electrodes to MCDI-1 and MCDI-2 with one pristine electrode and the other with positively shifted E_{PZC} leads to remarkably different performances. Beyond changes to pore structure and wettability, a better understanding of E_{PZC} in the context of CDI and MCDI can be integral to improving and preserving performance in capacitive deionization. Performance degradation in CDI experiments has been shown to be intricately linked to the E_{PZC}, and for the first time, it is also shown to affect performance in a membrane capacitive deionization operation as shown in the results presented in this work.

CONCLUSIONS

We present the performance evaluation of CDI and MCDI single cells configured symmetrically with a pair of pristine CX electrodes and asymmetrically with pristine CX and electrochemically oxidized CX electrodes. For the symmetrically configured CDI cell, post-testing evaluation of used electrodes showed shifting of the E_{PZC} at the anode to more positive potentials which increases co-ion expulsion and degrades long-term performance. Reduced anode E_{PZC} mobility was seen with MCDI, which showed a more stable performance after 50 h of operation. Asymmetric CDI configuration showed strongly contrasting results depending on the location of E_{PZC}, such that degraded and inverted performance was observed when E_{PZC}s were in the working domains of the electrodes and there was a boost when out of the domains. MCDI with E_{PZC}s in the working domain still showed desalination, albeit reduced in comparison to MCDI with symmetrically configured electrodes. The asymmetric MCDI cell with E_{PZC}s outside the working domain displayed the best performance result of all the tested cells due to having E_{PZC}s located to enhance the appropriate ion excess and the membrane in-place to reject expelled co-ions from accessing the bulk and mitigate electrochemical side reactions. The leveraging of electro-oxidized CDI electrodes is demonstrated here for the first time to possess synergistic benefits to improving desalination, when appropriately integrated with ion-exchange membranes.

ASSOCIATED CONTENT

Supporting Information

Information and data on the response of dissolved O_2 content and pH and the accumulation of charge in CDI and MCDI cells during operation between 1.2 and 0 V; FTIR analysis of pristine, used cathode, and used anode electrodes. This material is available free of charge via the Internet at http://pubs.acs.org/.

AUTHOR INFORMATION

Corresponding Authors

*E-mail: james.landon@uky.edu.
*E-mail: Kunlei.Liu@uky.edu.

Notes

The authors declare no competing financial interest.

ACKNOWLEDGMENTS

The authors are thankful for the support of the State of Wyoming Advanced Conversion Technologies Task Force for supporting this research.

REFERENCES

(1) Garcia-Quismondo, E.; Gomez, R.; Vaquero, F.; Cudero, A. L.; Palma, J.; Anderson, M. New Testing Procedures of a Capacitive Deionization Reactor. *Phys. Chem. Chem. Phys.* **2013**, *15*, 7648−7656.
(2) Micale, G.; Cipollina, A.; Rizzuti, L. Seawater Desalination for Freshwater Production. In *Seawater Desalination*, Micale, G., Rizzuti, L., Cipollina, A., Eds.; Springer: Berlin, 2009; pp 1−15.
(3) Kalogirou, S. A. Seawater Desalination Using Renewable Energy Sources. *Prog. Energy Combust. Sci.* **2005**, *31*, 242−281.

(4) Suss, M. E.; Baumann, T. F.; Bourcier, W. L.; Spadaccini, C. M.; Rose, K. A.; Santiago, J. G.; Stadermann, M. Capacitive Desalination with Flow-Through Electrodes. *Energy Environ. Sci.* **2012**, *5*, 9511−9519.
(5) Zhao, R.; Porada, S.; Biesheuvel, P. M.; van der Wal, A. Energy Consumption in Membrane Capacitive Deionization for Different Water Recoveries and Flow Rates, and Comparison with Reverse Osmosis. *Desalination* **2013**, *330*, 35−41.
(6) Anderson, M. A.; Cudero, A. L.; Palma, J. Capacitive Deionization as an Electrochemical Means of Saving Energy and Delivering Clean Water. Comparison to Present Desalination Practices: Will It Compete? *Electrochim. Acta* **2010**, *55*, 3845−3856.
(7) Andelman, M. Flow Through Capacitor Basics. *Sep. Purif. Technol.* **2011**, *80*, 262−269.
(8) Avraham, E.; Bouhadana, Y.; Soffer, A.; Aurbach, D. Limitation of Charge Efficiency in Capacitive Deionization I. On the Behavior of Single Activated Carbon. *J. Electrochem. Soc.* **2009**, *156*, 95−99.
(9) Farmer, J. C.; Fix, D. V.; Mack, G. V.; Pekala, R. W.; Poco, J. F. Capacitive Deionization of NaCI and $NaNO_3$ Solutions with Carbon Aerogel Electrodes. *J. Electrochem. Soc.* **1996**, *143*, 159−169.
(10) Gao, X.; Omosebi, A.; Landon, J.; Liu, K. Enhancement of Charge Efficiency for a Capacitive Deionization Cell Using Carbon Xerogel with Modified Potential of Zero Charge. *Electrochem. Commun.* **2014**, *39*, 22−25.
(11) Jia, B.; Zou, L. Graphene Nanosheets Reduced by a Multi-Step Process as High-Performance Electrode Material for Capacitive Deionisation. *Carbon* **2012**, *50*, 2315−2321.
(12) Park, B.-H.; Kim, Y.-J.; Park, J.-S.; Choi, J. Capacitive Deionization Using a Carbon Electrode Prepared with Water-Soluble Poly (Vinyl Alcohol) Binder. *J. Ind. Eng. Chem.* **2011**, *17*, 717−722.
(13) Porada, S.; Zhao, R.; van der Wal, A.; Presser, V.; Biesheuvel, P. M. Review on the Science and Technology of Water Desalination by Capacitive Deionization. *Prog. Mater. Sci.* **2013**, *58*, 1388−1442.
(14) Biesheuvel, P. M.; van der Wal, A. Membrane Capacitive Deionization. *J. Membr. Sci.* **2010**, *346*, 256−262.
(15) Kim, J.-S.; Choi, J.-H. Fabrication and Characterization of a Carbon Electrode Coated with Cation-Exchange Polymer for the Membrane Capacitive Deionization Applications. *J. Membr. Sci.* **2010**, *355*, 85−90.
(16) Lee, J.-Y.; Seo, S.-J.; Yun, S.-H.; Moon, S.-H. Preparation of Ion Exchanger Layered Electrodes for Advanced Membrane Capacitive Deionization (MCDI). *Water Res.* **2011**, *45*, 5375−5380.
(17) Li, H.; Zou, L. Ion-Exchange Membrane Capacitive Deionization: A New Strategy for Brackish Water Desalination. *Desalination* **2011**, *275*, 62−66.
(18) Zhao, Y.; Wang, Y.; Wang, R.; Wu, Y.; Xu, S.; Wang, J. Performance Comparison and Energy Consumption Analysis of Capacitive Deionization and Membrane Capacitive Deionization Processes. *Desalination* **2013**, *324*, 127−133.
(19) Kim, Y.-J.; Choi, J.-H. Enhanced Desalination Efficiency in Capacitive Deionization with an Ion-Selective Membrane. *Sep. Purif. Technol.* **2010**, *71*, 70−75.
(20) Biesheuvel, P. M.; Zhao, R.; Porada, S.; Van der Wal, A. Theory of Membrane Capacitive Deionization Including the Effect of the Electrode Pore Space. *J. Colloid Interface Sci.* **2011**, *360*, 239−248.
(21) Jeon, S.-i.; Park, H.-r.; Yeo, J.-g.; Yang, S.; Cho, C. H.; Han, M. H.; Kim, D. K. Desalination Via a New Membrane Capacitive Deionization Process Utilizing Flow-Electrodes. *Energy Environ. Sci.* **2013**, *6*, 1471−1475.
(22) Li, H.; Gao, Y.; Pan, L.; Zhang, Y.; Chen, Y.; Sun, Z. Electrosorptive Desalination by Carbon Nanotubes and Nanofibres Electrodes and Ion-Exchange Membranes. *Water Res.* **2008**, *42*, 4923−4928.
(23) Bouhadana, Y.; Avraham, E.; Noked, M.; Ben-Tzion, M.; Soffer, A.; Aurbach, D. Capacitive Deionization of NaCl Solutions at Non-Steady-State Conditions: Inversion Functionality of the Carbon Electrodes. *J. Phys. Chem. C* **2011**, *115*, 16567−16573.
(24) Cohen, I.; Avraham, E.; Bouhadana, Y.; Soffer, A.; Aurbach, D. Long Term Stability of Capacitive De-Ionization Processes for Water Desalination: The Challenge of Positive Electrodes Corrosion. *Electrochim. Acta* **2013**, *106*, 91−100.
(25) Avraham, E.; Noked, M.; Bouhadana, Y.; Soffer, A.; Aurbach, D. Limitations of Charge Efficiency in Capacitive Deionization Processes III: The Behavior of Surface Oxidized Activated Carbon Electrodes. *Electrochim. Acta* **2010**, *56*, 441−447.
(26) Leonard, K. C.; Genthe, J. R.; Sanfilippo, J. L.; Zeltner, W. A.; Anderson, M. A. Synthesis and Characterization of Asymmetric Electrochemical Capacitive Deionization Materials Using Nanoporous Silicon Dioxide and Magnesium Doped Aluminum Oxide. *Electrochim. Acta* **2009**, *54*, 5286−5291.
(27) Landon, J.; Gao, X.; Kulengowski, B.; Neathery, J. K.; Liu, K. Impact of Pore Size Characteristics on the Electrosorption Capacity of Carbon Xerogel Electrodes for Capacitive Deionization. *J. Electrochem. Soc.* **2012**, *159*, 1861−1866.
(28) Kim, S. H. Immersion Method for the Potential of Zero Charge Determination. Electrode Pretreatment. *J. Phys. Chem.* **1973**, *77*, 2787−2789.
(29) Bard, A. J.; Zoski, C. *Electroanalytical Chemistry: A Series of Advances*; Taylor & Francis: Boca Raton, FL, 2011.
(30) Landolt, D. *Corrosion and Surface Chemistry of Metals*; CRC Press LLC: Boca Raton, FL, 2007.
(31) Lust, E.; Nurk, G.; Jänes, A.; Arulepp, M.; Nigu, P.; Möller, P.; Kallip, S.; Sammelselg, V. Electrochemical Properties of Nanoporous Carbon Electrodes in Various Nonaqueous Electrolytes. *J. Solid State Electrochem.* **2003**, *7*, 91−105.
(32) Suss, M. E.; Baumann, T. F.; Worsley, M. A.; Rose, K. A.; Jaramillo, T. F.; Stadermann, M.; Santiago, J. G. Impedance-Based Study of Capacitive Porous Carbon Electrodes with Hierarchical and Bimodal Porosity. *J. Power Sources* **2013**, *241*, 266−273.
(33) Bouhadana, Y.; Ben-Tzion, M.; Soffer, A.; Aurbach, D. A Control System for Operating and Investigating Reactors: The Demonstration of Parasitic Reactions in the Water Desalination by Capacitive De-Ionization. *Desalination* **2011**, *268*, 253−261.
(34) Ogumi, Z.; Takehara, Z.; Yoshizawa, S. Gas Permeation in SPE Method I. Oxygen Permeation Through Nafion and Neosepta. *J. Electrochem. Soc.* **1984**, *131*, 769−773.
(35) Ban, S.; Zhang, J.; Zhang, L.; Tsay, K.; Song, D.; Zou, X. Charging and Discharging Electrochemical Supercapacitors in the Presence of Both Parallel Leakage Process and Electrochemical Decomposition of Solvent. *Electrochim. Acta* **2013**, *90*, 542−549.